

${}^6\text{Li} + {}^6\text{Li}$ Scattering at $E_{\text{c.m.}} = 5\text{--}17$ MeV*

H. T. Fortune,[†] G. C. Morrison, and R. H. Siemssen

Argonne National Laboratory, Argonne, Illinois 60439

(Received 21 December 1970)

For the elastic scattering of ${}^6\text{Li} + {}^6\text{Li}$, excitation functions at c.m. angles of 60, 70, 80, and 90° have been studied in the c.m. energy range 5–17 MeV, and angular distributions have been measured at c.m. energies of 6, 10, and 14 MeV. The excitation functions are relatively featureless, with a broad gross-structure peak at 90° centered around 13 MeV. Good fits to individual angular distributions are obtained with the optical model and, except for the highest energies studied, parametrized phase-shift calculations. These calculations, however, do not correctly reproduce the energy dependence of the data. The single most outstanding conclusion from the present analysis is that ${}^6\text{Li} + {}^6\text{Li}$ is dominated by absorption, and this dominance leads to scattering behavior very different from that found for other heavy ions.

I. INTRODUCTION

The scattering of heavy ions has attracted much renewed interest recently with the observation of pronounced gross structure in the ${}^{16}\text{O} + {}^{16}\text{O}$ elastic scattering excitation functions.^{1, 2} In particular, it has been suggested^{3–5} that the heavy-ion-nucleus potential is of the molecular type (i.e., very shallow and with a repulsive core), and possible parallels with the $\alpha + \alpha$ scattering⁶ have been emphasized. For $\alpha + \alpha$ scattering a unique set of phase shifts exists for incident energies from 0 to approximately 35 MeV, and from these phase shifts l -dependent real potentials with a repulsive core have been derived by various authors.⁶ Since ${}^6\text{Li} + {}^6\text{Li}$ is the next heaviest system of identical particles amenable to a scattering study, such an investigation would seem to be of special interest.

There are, however, some significant differences between the $\alpha + \alpha$ and the ${}^6\text{Li} + {}^6\text{Li}$ systems. Whereas for the $\alpha + \alpha$ scattering only even partial waves contribute, the spin-1 ground state of ${}^6\text{Li}$ removes this restriction for ${}^6\text{Li} + {}^6\text{Li}$. Also, because of the tight binding of the α particle, there are no open particle-breakup channels for $\alpha + \alpha$ below about 20-MeV excitation in ${}^4\text{He}$, and consequently the scattering can be fitted with purely real phase shifts for energies below the threshold for the opening of inelastic channels. Contrary to this, ${}^6\text{Li}$ is known to disintegrate easily ($E_{\text{sep}} = 1.47$ MeV), and therefore one may expect absorption due to breakup to be important even at very low incident energies.

We wish to report here a study of the ${}^6\text{Li} + {}^6\text{Li}$ scattering, in which we have measured both excitation functions and angular distributions. The data have been analyzed with the optical model and with parametrized phase-shift models. A preliminary account of the data and of the experimental method

has already been published.⁷ In addition to the present work, ${}^6\text{Li} + {}^6\text{Li}$ elastic scattering has been studied at other laboratories.^{8, 9}

II. EXPERIMENTAL METHOD

Beams of ${}^6\text{Li}^{++}$ in the energy range from 10 to 34 MeV were accelerated with the Argonne FN tandem accelerator. ${}^6\text{Li}^-$ ions were obtained by bombarding lithium vapor in the exchange canal with H^+ ions from the duoplasmatron ion source. Typical electrical currents on target ranged between 10 and 30 nA. Targets were produced by evaporating ${}^6\text{LiF}$ layers of approximately $100\text{-}\mu\text{g}/\text{cm}^2$ thickness onto self-supporting $20\text{-}\mu\text{g}/\text{cm}^2$ carbon films.

For particle identification, kinematic coincidences between the scattered ion and the recoiling target nucleus were employed. For elastically scattered identical particles the angle between the scattered ion and the recoil is always 90°, independent of the scattering angle. The experiment makes use of a computer-controlled multiple-detector array.¹⁰ A total of eight rectangular large-area detectors (i.e., four coincident pairs of detectors) were mounted onto two remotely controlled arms of the Argonne 70-in. scattering chamber.¹¹ Apertures in front of the angle-defining detectors were kinematically curved; the apertures of the conjugate detectors were approximately twice as wide as those of the angle-defining slits to ensure complete overlap. The angular resolution was $\pm 0.5^\circ$ in the laboratory frame, i.e., $\pm 1^\circ$ in the center-of-mass frame. For the measurements at forward angles ($\theta_{\text{lab}} < 40^\circ$), a single detector was employed.

Spectra from the coincident detector pairs were stored two dimensionally in 64×128 -channel arrays. This allows setting tight energy windows over the peaks of interest after the data have been

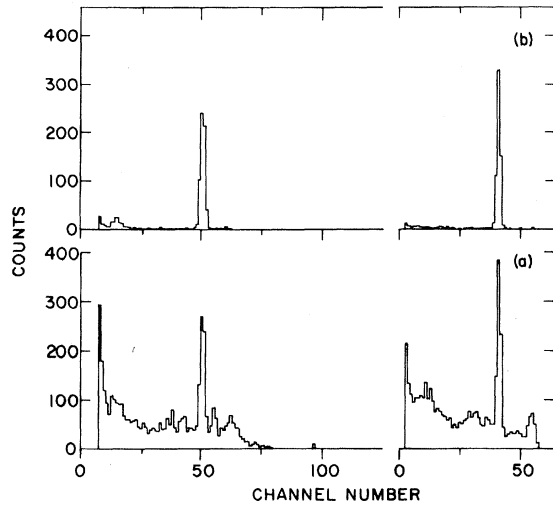


FIG. 1. Two-dimensional ${}^6\text{Li} + {}^6\text{Li}$ coincidence spectra of 128×64 channels projected onto the x and y axes (a) without and (b) with "energy windows" set on the elastic peak.

taken. While this technique has also proved useful in several other studies of heavy-ion elastic scattering in this laboratory, this feature is espe-

cially important for the investigation of the ${}^6\text{Li} + {}^6\text{Li}$ scattering in which the spectra contain a sizable coincident background from three-body break-up. In Fig. 1, typical coincident ${}^6\text{Li} + {}^6\text{Li}$ scattering spectra are shown for two conjugate detectors. The lower spectra show the total coincidences without energy windows set. The upper spectra present the same data with energy windows set over the peaks of interest, i.e., they are "slices" projected out of the two-dimensional spectra.

Absolute cross sections were obtained by simultaneously measuring the ${}^6\text{Li} + {}^6\text{Li}$ and the ${}^{19}\text{F} + {}^6\text{Li}$ scattering at laboratory energies of 12, 20, and 28 MeV with a ${}^6\text{LiF}$ target, and then normalizing the ${}^6\text{Li} + {}^6\text{Li}$ data to the ${}^{19}\text{F} + {}^6\text{Li}$ cross sections. The ${}^{19}\text{F} + {}^6\text{Li}$ absolute cross sections in turn were obtained by comparison at the same energies with the $\text{Ca} + {}^6\text{Li}$ scattering from a CaF_2 target, in which case the $\text{Ca} + {}^6\text{Li}$ data had been found to be pure Coulomb scattering at the most forward angles. Absolute cross sections derived for ${}^6\text{Li} + {}^6\text{Li}$ by this method are believed to be accurate to $\pm 15\%$.

III. RESULTS AND DISCUSSION

The data are presented in Figs. 2 and 3. Figure

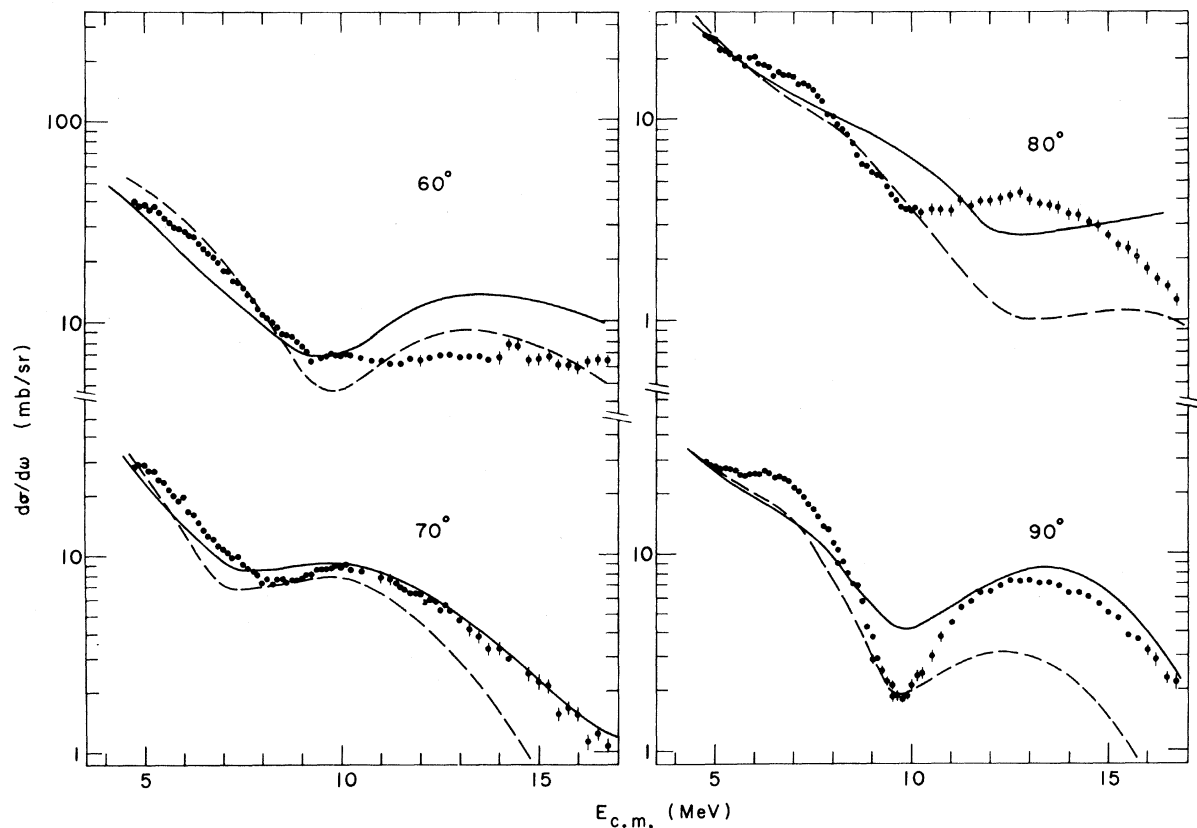


FIG. 2. ${}^6\text{Li} + {}^6\text{Li}$ elastic scattering excitation functions measured at 60, 70, 80, and 90°. The solid and the dashed curves are the optical-model predictions obtained from Pot. A and Pot. B, respectively; Their parameters are listed in Table I.

2 shows the 60, 70, 80, and 90° excitation functions from $E_{\text{c.m.}} = 5-17$ MeV, and Fig. 3 presents the angular distributions measured at $E_{\text{c.m.}} = 6, 10,$ and 14 MeV. Since ${}^6\text{Li} + {}^6\text{Li}$ involves the scattering of identical particles, the angular distributions are symmetric about 90°. Therefore no data have been measured beyond 100°. Elastic scattering measurements performed at Heidelberg⁸ overlap the present data for c.m. energies below 9 MeV; there is good agreement in the shape of the excitation functions although their absolute cross sections are higher than ours by about a factor 1.3-1.4. Nagatani *et al.*⁹ measured elastic scattering at 16 MeV; at large angles, where their angular distribution overlaps our excitation curves, their absolute cross sections are lower by about a factor of 10. This discrepancy is not understood.

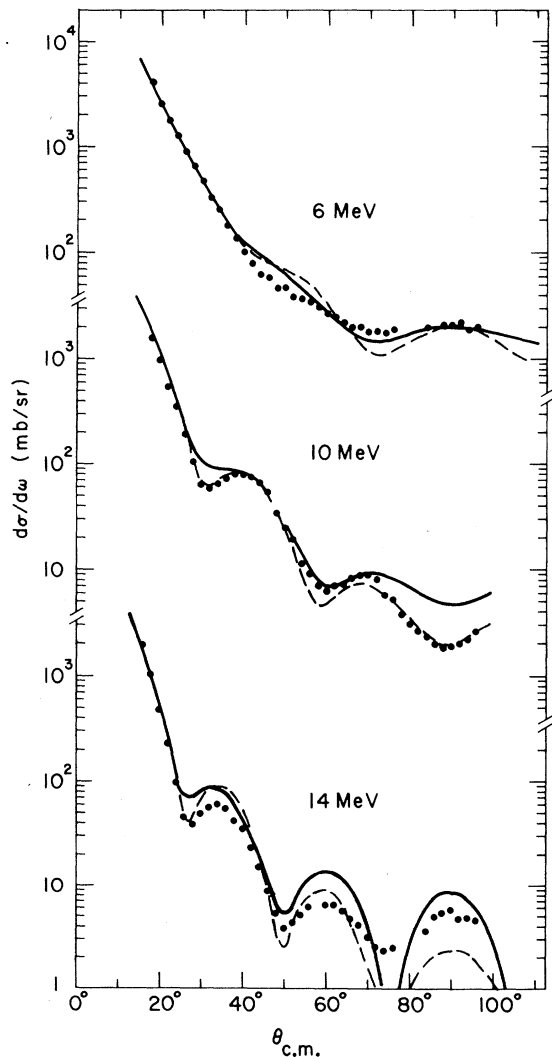


FIG. 3. ${}^6\text{Li} + {}^6\text{Li}$ elastic scattering angular distributions measured at $E_{\text{c.m.}} = 6, 10,$ and 14 MeV. The solid and dashed curves are as described in Fig. 2.

The angular distributions (Fig. 3) appear to vary slowly with increasing energy. The excitation functions are rather featureless except for a gross-structure peak at 90° centered around 13 MeV, and for some broad and not very pronounced structure in the 70 and 80° excitation functions. The approximately 7-MeV width of this structure is much broader than the approximately 3-MeV width found in the ${}^{16}\text{O} + {}^{16}\text{O}$ scattering (at somewhat higher c.m. energies). This feature can readily be understood by the fact that the maximum l value that contributes to the scattering is less for ${}^6\text{Li} + {}^6\text{Li}$ than for ${}^{16}\text{O} + {}^{16}\text{O}$, even at the same c.m. energy.

We have analyzed the data both with the optical model and with parametrized phase shifts. These calculations were done with the extensively modified¹² Argonne version of the optical-model program ABACUS.¹³ The calculations take the spin-1 identical-particle nature of the ${}^6\text{Li} + {}^6\text{Li}$ scattering into account. Woods-Saxon form factors were used for both the real and the imaginary potentials. It was generally necessary to employ different geometrical parameters for the real and the imaginary well. No spin-orbit potential was included.

It is found that individual angular distributions can be well fitted by optical-model calculations. However, none of the parameter sets obtained from these calculations correctly predicts the energy dependence of the data. This is shown in Figs. 2 and 3, where optical-model calculations performed with two different sets of parameters are compared with the data. Their parameters are listed in Table I. The dashed curves were obtained from the potential (Pot. B of Table I) that gave best agreement with the 10-MeV data. The solid curves were calculated from the potential that gives the most reasonable account of the data over the whole energy range, although it does not yield the best fit at any one energy. This potential (Pot. A of Table I) was derived from the best-fit potential at 14 MeV by increasing the diffuseness a_1 of the real well.

The over-all agreement of the optical-model calculations with the angular distributions in Fig. 3 is perhaps acceptable, but the poorer agreement with the excitation functions (Fig. 2) is not. Notably, in the 80° excitation function, the data show a peak

TABLE I. Optical-model parameters. The subscripts 1 and 2 refer to the real and imaginary terms, respectively.

Pot.	V (MeV)	R_1 (F)	a_1 (F)	W (MeV)	R_2 (F)	a_2 (F)	R_C (F)
A	17.0	5.0	0.25	80.0	1.10	1.22	4.8
B	11.7	5.0	0.46	6.9	5.46	0.728	4.8

in the energy range 10–14 MeV, while the calculations have a dip there. Very extensive optical-model searches and scans did not yield better results. In fact, no calculation was able to yield a peak in this energy region in both the 80 and 90° excitation functions simultaneously. Allowing for linear energy dependences of the real and imaginary potential strengths did not significantly improve the fits to the excitation functions.

The inability to achieve an over-all fit to the excitation functions is also reflected in our failure to fit the three sets of angular distributions simultaneously. In fact, no potential could be found to fit both the 10- and 14-MeV angular distributions, even though good fits to *either* of these two energies and the 6-MeV data were possible. Of course, this latter feature may reflect the comparatively poor discrimination afforded by the relatively smooth angular distribution at 6 MeV.

An inspection of the optical-model parameters (Table I) shows that the Pot. A set has a very small diffuseness $a_1 = 0.25$ F for the real potential. (The best fit at 14 MeV was obtained with an even smaller value, $a_1 = 0.1$ F.) Keeping a_1 fixed at a larger value in the range 0.5–1.2 F and allowing

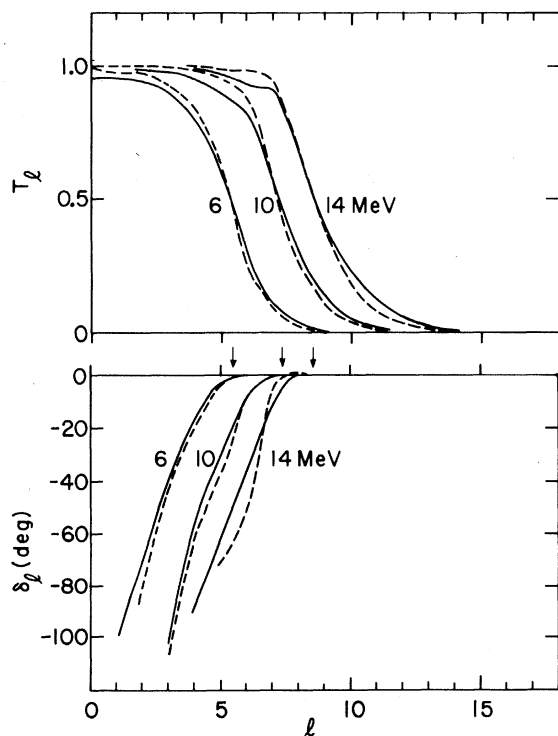


FIG. 4. Transmission coefficients T_l and (real) phase shifts δ_l corresponding to optical-model predictions for ${}^6\text{Li} + {}^6\text{Li}$ scattering at c.m. energies of 6, 10, and 14 MeV. The solid and dashed curves correspond to Pot. A and Pot. B, respectively. The arrows indicate the l values for which $T_l = 0.5$ for the three c.m. energies.

all the other parameters to vary produced poorer fits. This result is difficult to understand in view of the loose binding of ${}^6\text{Li}$, which would suggest a rather diffuse surface for this nucleus. Of interest also is the shape of the imaginary potential in set A, which is approximately that of a Gaussian centered at zero radius. It roughly resembles the shape of the “microscopic” potential obtained by folding the charge distributions of the two nuclei into each other and assuming a contact interaction. However, calculations with such “microscopic” imaginary form factors gave significantly poorer fits. This apparent sensitivity to the shape of the imaginary potential contrasts sharply with the insensitivity found for the ${}^{16}\text{O}$ scattering.^{14,15} Despite these difficulties in obtaining a consistent set of parameters over the whole energy range, some general features that emerge from the optical-model calculations appear to be independent of the parametrizations chosen.

(i) All the optical-model calculations consistently yield very shallow real potentials, independent of the starting parameters in the search. With a real radius $R_1 = 4.6$ F and a diffuseness $a_1 = 0.49$ F, independent searches on all three angular distributions gave best fits for real-potential depths in the neighborhood of 10 MeV. Thus the ${}^6\text{Li} + {}^6\text{Li}$ scattering has the shallow real-potential characteristic of ${}^{16}\text{O}$ scattering from light nuclei. However, in the ${}^{16}\text{O}$ scattering a shallow real potential V appeared necessary only in fitting the energy dependence of the data and was not obviously preferred from an analysis of individual angular distributions. In the ${}^6\text{Li}$ scattering, an increase in V leads to a shrinking of the diffraction pattern and a worsening of the fit.

(ii) An inspection of the phase shifts from the best-fit optical-model calculations indicates that the radius at which absorption sets in is larger than that for which the effects of the real nuclear potential are felt by the interacting particles. In Fig. 4, both the transmission coefficients T_l and the nuclear phase shifts δ_l calculated with the potentials of Table I are plotted versus orbital angular momentum l . On this plot it can be seen that the nuclear phase shift remains approximately zero until the transmission coefficient is up to about 0.7. The phase shift then becomes negative. This behavior is again in contrast to that typically found in the scattering of other heavy ions such as ${}^{16}\text{O}$, for which the nuclear phase shift for a given l differs from zero as soon as absorption sets in for this partial wave, i.e., as soon as the transmission coefficient is nonzero for that l value. Also, in the ${}^{16}\text{O}$ scattering the phase shifts typically first become positive as the effects of the attractive potential are felt.

The peculiar behavior of the ${}^6\text{Li} + {}^6\text{Li}$ phase shifts (consistently found with all potentials that fit the data) probably reflects the fact that the ${}^6\text{Li} + {}^6\text{Li}$ scattering is indeed dominated by absorption. It was therefore tempting to try to fit the data with purely imaginary potentials. Simply setting $V = 0$ in the potentials that had given reasonable fits and then using these parameters as starting values in a search on the imaginary potential W generally did not lead to acceptable fits. It was possible, however, to find purely imaginary potentials that could reproduce both the 6- and 14-MeV angular distributions. These best fits [Fig. 5(a)] resulted in very different geometrical parameters – specifically, a much larger imaginary radius R_2 and a much smaller diffuseness a_2 than were obtained for the best-fit potential with $V \neq 0$. In fact, the best fits were obtained with an almost square-well imaginary potential, a result again surprising in view of the diffuse surface of ${}^6\text{Li}$. Attempts to obtain fits with more conventional geometrical parameters and a purely imaginary well led to significantly poorer fits.

If one next looks at the phase shift obtained from the potentials of Table I with $V = 0$, one finds for the 14-MeV case that δ_l for large l is no longer zero (dashed curve in Fig. 6) but positive. Thus the effect of the real potential seems to be to cancel out some of the effects of the imaginary potential, thereby making the *interaction* purely absorptive for grazing collisions. It is obviously then of interest to examine the goodness of the fits that can be obtained with a purely absorptive interaction, i.e., with $\delta_l = 0$ for all l . The result of such a phase-shift calculation with the McIntyre parametrization¹⁶ is shown in Fig. 5(b), and the corresponding best-fit parameters are listed in Table II. The fits are seen to be reasonable for 6 and 10 MeV and even reproduce the 14-MeV data for angles out to about 70° , again pointing up the important role of absorption in the scattering. We also attempted to fit the angular distributions with calculations based on the full parametrized phase-shift model ($\delta_l \neq 0$). The best fit obtained with either the McIntyre¹⁶ or the Conzett¹⁷ parametrizations was comparable with those from the optical-

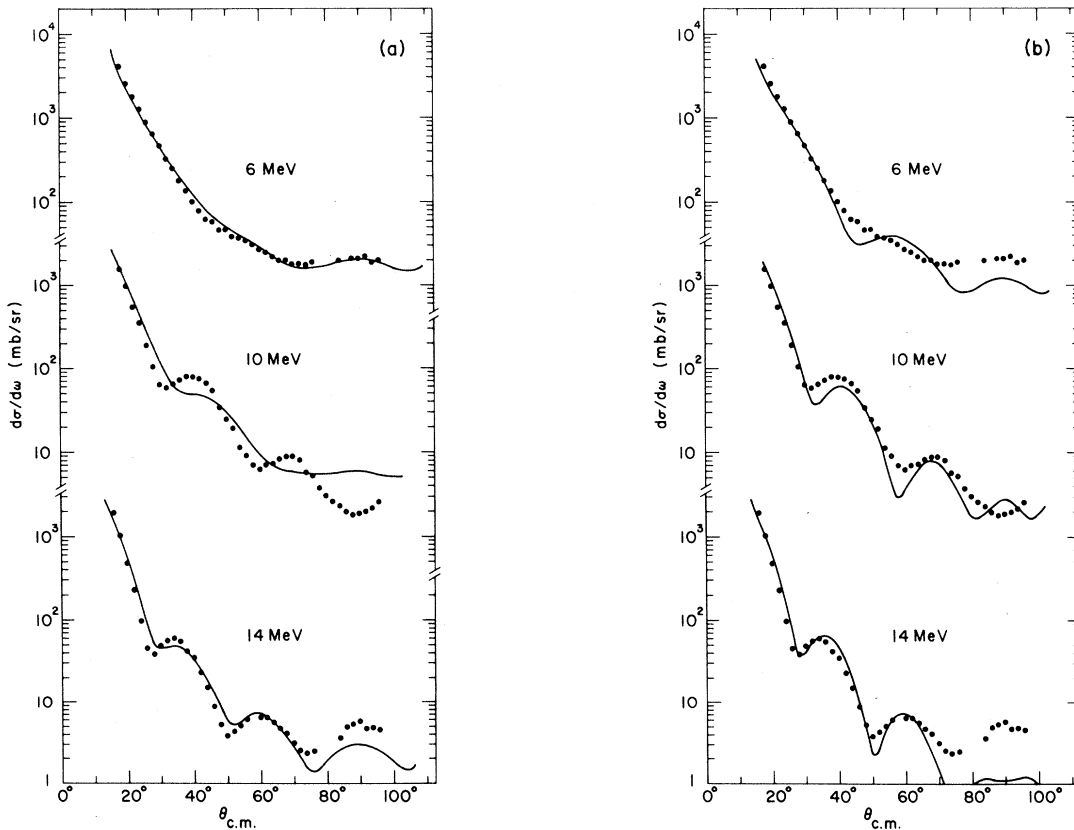


FIG. 5. Comparison between calculations and the ${}^6\text{Li} + {}^6\text{Li}$ elastic scattering angular distributions. (a) Optical-model calculations. The potential used in calculating these curves was purely imaginary (i.e., $V = 0$) and its parameters were $R_2 = 6.30$ F, $a_2 = 0.248$ F, and $W = 3.5$ MeV. (b) Parametrized-phase-shift-model calculations. The curves were calculated with $\delta_l = 0$ for all l , and the potential parameters were as listed in Table II.

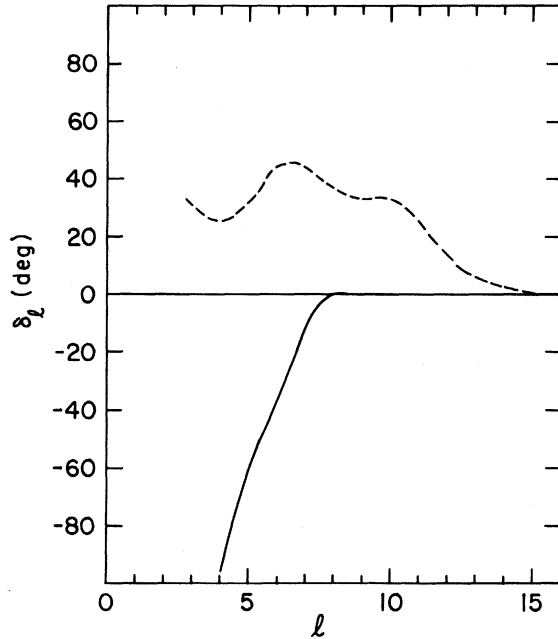


FIG. 6. Real phase shift δ_l for $E_{c.m.} = 14$ MeV corresponding to the optical-model prediction (Pot. A). The dashed curve was calculated with $V=0$, the solid curve with $V \neq 0$.

model calculations for the 6- and 10-MeV angular distributions; for the 14-MeV data, neither of the parametrized-phase-shift-model calculations was as successful. This is not surprising, since the optical-model best fit to the 14-MeV data requires an irregular variation in the transmission coefficient T_l (Fig. 4) which conflicts with the smooth l dependence assumed in the parametrized phase-shift model.

Attempts to fit the individual angular distributions with purely repulsive real potentials were unsuccessful. Similarly, all attempts to obtain improved over-all fits were unsuccessful when a repulsive core of Gaussian shape was added to the attractive real potential.

IV. CONCLUSIONS

The ${}^6\text{Li} + {}^6\text{Li}$ scattering has been studied in the energy range from 5 to 17 MeV. Extensive optical-model calculations were able to reproduce individual angular distributions but did not succeed in

TABLE II. Parameters of the parametrized-phase-shift-model calculation in which the scattering matrix element S_l is related (Ref. 16) to l_A and Δl_A by the expression $S_l = [1 + e^{(l_A - l)/\Delta l_A}]^{-1}$.

E (MeV)	l_A	Δl_A
6	4.34	0.296
10	6.35	0.518
12	7.42	0.660

correctly predicting the energy dependence of the data. These difficulties may well be due to some complicated energy dependence in the ${}^6\text{Li} + {}^6\text{Li}$ potential, or to an l dependence such as is observed for $\alpha + \alpha$. However, a meaningful exploration of these possibilities would require a much more extensive collection of data than is presently available.

Despite these difficulties, however, one important conclusion seems justified. In contrast to $\alpha + \alpha$, and indeed to all other heavy-ion scattering so far studied, the ${}^6\text{Li} + {}^6\text{Li}$ scattering appears to be dominated by absorption. This may be inferred from the behavior of the phase shifts, which is strikingly different from that found in other heavy-ion analyses and appears to indicate that at a given energy there is absorption but no significant nuclear distortion of higher partial waves. A further indication is that apparently the only role of the real potential in ${}^6\text{Li} + {}^6\text{Li}$ scattering is to cancel out some of the effects of the imaginary potential; in contrast, the real potential largely determines the character of the scattering of ${}^{16}\text{O}$. While it seems reasonable to ascribe the dominance of absorption to the loosely bound nature of ${}^6\text{Li}$ and the consequent breakup that removes it from the incident beam, studies of other loosely bound systems would seem highly desirable.

ACKNOWLEDGMENTS

We are grateful to Dr. J. E. Monahan for helpful discussions. The assistance of R. Adams in the data analysis, of S. Zawadski in the ABACUS programming, and of the operating crew of the Argonne tandem Van de Graaff is also much appreciated.

*Work performed under the auspices of the U. S. Atomic Energy Commission.

†Present address: University of Pennsylvania, Philadelphia, Pennsylvania 19104.

¹R. H. Siemssen, J. V. Maher, A. Weidinger, and D. A. Bromley, Phys. Rev. Letters **19**, 968 (1967); **20**, 175(E) (1968).

²J. V. Maher, M. W. Sachs, R. H. Siemssen, A. Weidinger, and D. A. Bromley, Phys. Rev. **188**, 1665 (1969).

³B. Block and F. B. Malik, Phys. Rev. Letters **19**, 239 (1967); R. J. Munn, B. Block, and F. B. Malik, *ibid.* **21**, 159 (1968).

⁴W. Scheid, R. Ligensa, and W. Greiner, Phys. Rev. Letters **21**, 1479 (1968); W. Scheid and W. Greiner, Z.

Physik **226**, 364 (1969).

⁵K. A. Brueckner, J. R. Buchler, and M. M. Kelly, Phys. Rev. **173**, 944 (1968).

⁶S. A. Afzal, A. A. Z. Ahmad, and S. Ali, Rev. Mod. Phys. **41**, 247 (1969), and references therein.

⁷G. C. Morrison, H. T. Fortune, and R. H. Siemssen, in *Proceedings of the International Conference on Nuclear Reactions Induced by Heavy Ions, Heidelberg, Germany, 15-18 July 1969*, edited by R. Bock and W. R. Hering (North-Holland Publishing Company, Amsterdam, The Netherlands, 1970), p. 72.

⁸I. Dormehl, G. Gruber, K. Meier-Ewert, and K. Bethge, Jahresbericht 1969, Universität Heidelberg, p. 8.

⁹K. Nagatani, D. P. Boyd, P. F. Donovan, E. Beardsworth, and P. A. Assimakopoulos, Phys. Rev. Letters **24**, 675 (1970).

¹⁰R. H. Siemssen, H. T. Fortune, J. W. Tippie, and J. L. Yntema, in *Proceedings of the International Conference on Nuclear Reactions Induced by Heavy Ions* (see

Ref. 7), p. 174.

¹¹J. L. Yntema, U. S. Atomic Energy Agency Report No. CONF-690301, 1969 (unpublished), pp. 321-325.

¹²S. Zawadski, unpublished.

¹³E. H. Auerbach, Brookhaven National Laboratory Report No. BNL-6562 (unpublished).

¹⁴J. V. Maher, R. H. Siemssen, M. W. Sachs, A. Weidinger, and D. A. Bromley, in *Proceedings of the International Conference on Nuclear Reactions Induced by Heavy Ions* (see Ref. 7), p. 60.

¹⁵R. H. Siemssen, H. T. Fortune, A. Richter, and J. W. Tippie, to be published.

¹⁶J. A. McIntyre, K. H. Wang, and L. C. Becker, Phys. Rev. **117**, 1337 (1960).

¹⁷H. E. Conzett, A. Isoya, and E. Hadjimichael, in *Proceedings of the Third Conference on Reactions between Complex Nuclei*, edited by A. Ghiorso, R. M. Diamond, and H. E. Conzett (University of California Press, Los Angeles, California, 1963), p. 26.

Study of $p + \text{He}^3$ and $n + \text{H}^3$ Systems with the Resonating-Group Method*

I. Reichstein,† D. R. Thompson, and Y. C. Tang

School of Physics, University of Minnesota, Minneapolis, Minnesota 55455

(Received 14 December 1970)

The $p + \text{He}^3$ and $n + \text{H}^3$ systems are considered with the resonating-group method in the one-channel approximation. A purely central nucleon-nucleon potential which has different ranges in the singlet and triplet states is employed. The internal wave function of the three-nucleon cluster is a sum of two Gaussian functions, with its parameters adjusted to reproduce quite well the properties of the cluster. From the results obtained it is found that the agreement with experiment is quite satisfactory, although in the very low-energy region, detailed fit is not obtained, which is most probably due to the omission of the specific distortion effect in our calculation. An effective interaction between the clusters is also constructed. From this effective interaction it is concluded that the requirement of antisymmetry for the total wave function is very important. In particular, it creates an odd-even feature, wherein the effective potentials in the odd- l and even- l states are quite different.

I. INTRODUCTION

In two previous investigations^{1,2} single-channel resonating-group calculations have been performed using a nucleon-nucleon potential which has the feature of having different ranges in the singlet and triplet states and which yields a very good fit to the low-energy two-nucleon scattering data. These calculations were made on the $\alpha + \alpha^1$ and $\alpha + N^2$ scattering systems, where the low compressibility of the α particle and the high reaction thresholds provided us with an excellent opportunity to employ the one-channel approximation over a wide energy range. Excellent agreement with experiment was obtained in these calculations. In this study we will use the same central potential

to examine the $p + \text{He}^3$ and $n + \text{H}^3$ systems,³ as another step in our continual effort to study the few-nucleon problems with the resonating-group method. Here, however, it is expected that the results will be somewhat worse than those obtained in the $\alpha + \alpha$ and $\alpha + N$ cases; this is so, since the He^3 or the H^3 cluster is not as incompressible as the α cluster, and hence the use of a one-channel approximation, with the subsequent omission of the specific distortion effect, will result in some lack of detailed agreement with the experimental data especially in the very low-energy region.

In previous resonating-group calculations, the wave function used to describe the He^3 or the H^3 cluster has invariably been assumed to consist of a single-Gaussian function.⁴⁻⁶ With such a wave